scientific reports

Check for updates

OPEN

Quaternary functionalized mesoporous adsorbents for ultra-high kinetics of CO_2 capture from air

Tao Wang[1]✉, Xinru Wang[1], Chenglong Hou[1] & Jun Liu[2]

Obstacles to widespread deployments of direct air capture of CO_2 (DAC) lie in high material and energy costs. By grafting quaternary ammonium (QA) functional group to mesoporous polymers with high surface area, a unique DAC adsorbent with moisture swing adsorption (MSA) ability and ultra-high kinetics was developed in this work. Functionalization is designed for efficient delivery of QA group through mesopores to active substitution sites. This achieved ultra-high kinetics adsorbent with half time of 2.9 min under atmospheric environment, is the highest kinetics value reported among DAC adsorbents. A cyclic adsorption capacity of 0.26 mmol g^{-1} is obtained during MSA process. Through adsorption thermodynamics, it is revealed that adsorbent with uniform cylindrical pore structure has higher functional group efficiency and CO_2 capacity. Pore structure can also tune the MSA ability of adsorbent through capillary condensation of water inside its mesopores. The successful functionalization of mesoporous polymers with superb CO_2 adsorption kinetics opens the door to facilitate DAC adsorbents for large-scale carbon capture deployments.

Limiting global warming to less than 1.5 °C over preindustrial levels with limited or no overshoot projects the Negative Emission Technologies (NETs)[1], which is expected to remove CO_2 on the order of 100 Gt by midcentury[2]. As an important component of NETs portfolio, direct air capture (DAC) of CO_2 by chemicals has advantages of low environmental risk, convenient feedstock for CO_2 utilization and unlimited capacity in reducing atmospheric CO_2 level[3,4]. However, NETs are always challenged by low kinetics issues under the ultra-low CO_2 partial pressure of 40 Pa in air. Under this atmospheric environment, the rates of CO_2 uptake by photosynthesis and ocean absorption are on the order of 10^{-6} and 10^{-8} mol m^{-2} s^{-1}, respectively[5,6].

Kinetics of artificial material of DAC can be hundreds of times higher than that of natural process. Decades of sorbents development for flue gas capture provides various functional parts referenced to DAC, ranging from alkali hydroxides to solid amines[4,7]. As both functionalization and CO_2 adsorption need channels for molecule diffusion, porous DAC adsorbents have aroused extensive concerns. During functional group impregnation, researchers found that amine molecules are prone to first filling small pores (< 10 nm) due to their relatively high surface potential[8,9]. This would result in complete filling of pore channels and limiting CO_2 diffusion after functionalization, especially for adsorbents with microporous. To avoid this outcome, low functional group loading (e.g. < 9 mmol N g^{-1}) is suggested to keep a certain amount of mesopores (e.g. 1 cm^3 g^{-1} for aerogel[10], 0.35 cm^3 g^{-1} for mesoporous alumina[11]). In situ polymerization with amine-containing monomers, e.g., linear poly-L-alanine[8] or hyperbranched aminosilica[12], is also a preference for keeping the mesoporous structure of adsorbents.

Of particular interest to this work is chemically grafting quaternary ammonium (QA) groups on mesoporous material for DAC adsorption. The QA groups possess the ability of moisture swing adsorption (MSA) which employs water to trigger the desorption, rather than heat or electrical energy. Therefore, the MSA could have a lower energy consumption than temperature-swing adsorption (TSA) process[13]. The pore structures are introduced to MSA adsorbent in this work to enhance its molecular diffusivity. The grafting of QA cations with strong ionic bonding towards anions can avoid the overlap of functional groups inside mesopores[14]. Also, the mesopores can provide more surface area for functionalization, compared to macroporous supports[4,7,15,16] or cellulose fiber with limited pore structure[17]. This further provides sufficient channels for CO_2 diffusion and high efficiency ammonium sites for CO_2 to be captured. On the other hand, moisture swing adsorption (MSA) is known as

[1]State Key Laboratory of Clean Energy Utilization, College of Energy Engineering, Zhejiang University, Hangzhou 310027, People's Republic of China. [2]School of Electric Power, North China University of Water Resources and Electric Power, Zhengzhou 450045, People's Republic of China. ✉email: oatgnaw@zju.edu.cn

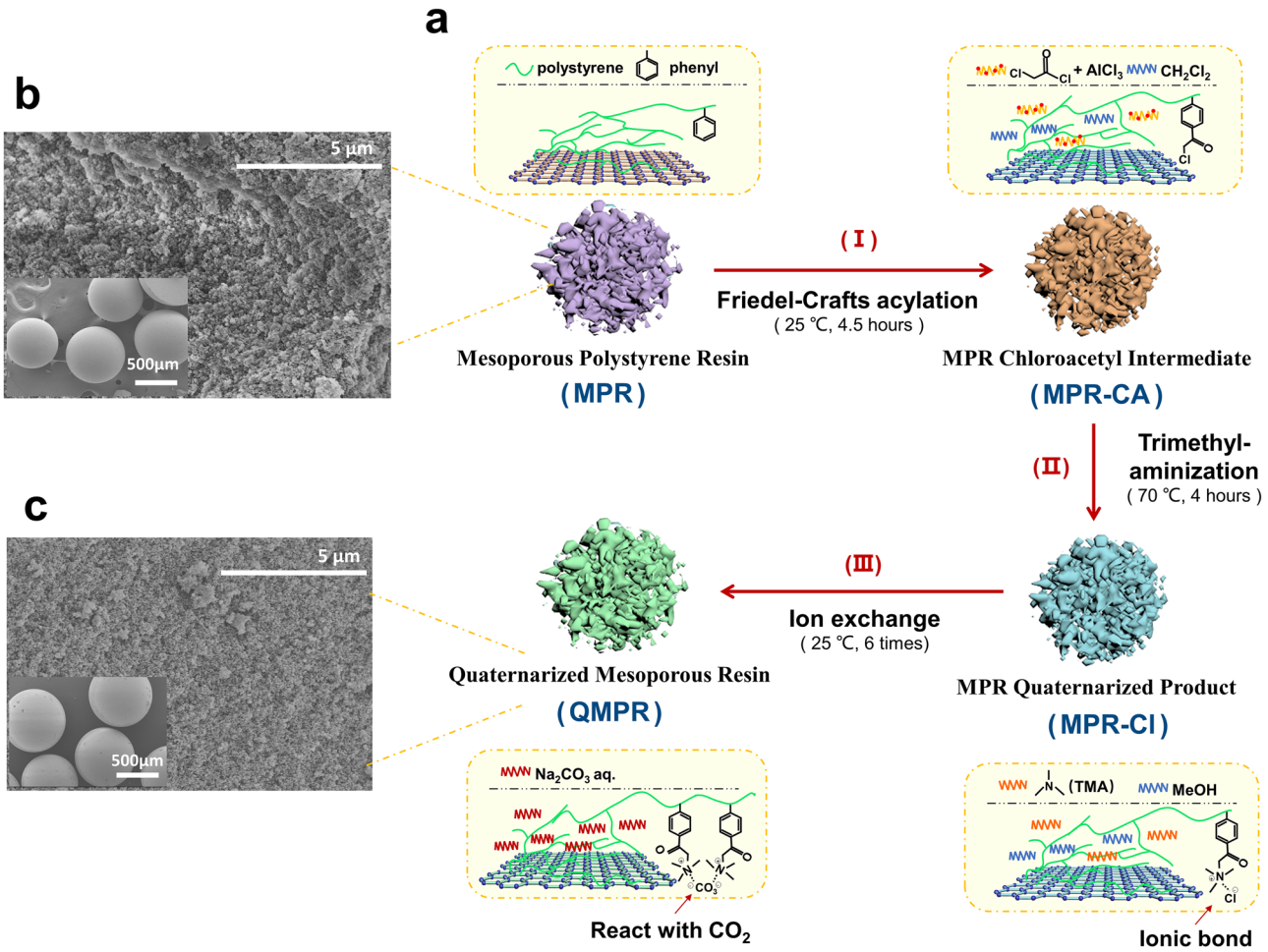

Figure 1. Fabrication and morphology of QMPRs. (**a**) Schematic illustration of QMPR adsorbents preparation through three-step process. (**b**,**c**) SEM images of the MPRs and QMPRs (**b** represents MPR-2, and **c** represents QMPR-2) including both particle and internal pore morphology.

water can distinctly alter the binding energy of QA ion pair to CO_2 through the Brønsted base mechanism[15,18]. Thus, water behavior in mesopores, such as diffusion and capillary condensation, will ultimately project on the performance of moisture swing adsorbents.

Results

Design and fabrication of QMPRs. Quaternary ammonium functionalized mesoporous adsorbents (QMPRs) are produced though a three-step process illustrated in Fig. 1a. Using this approach, three types of porous QMPRs based on MPRs with similar particle size (500–600 μm as shown in Fig. 1b,c) have been prepared (FTIR analysis and surface morphology are shown in Supplementary Fig. 1). During synthesis process, dichloromethane and methanol were selected as swelling agents, as they can overcome steric hindrance and permeate reagents into active substitution sites at a sufficiently swelled state[19]. Carbonate is selected as the counter anion to QA group to build a strong interaction with CO_2 in air[15].

Characterization of pore structure. N_2 adsorption and desorption isotherms of different MPRs are shown in Fig. 2a. All MPRs exhibit type IV isotherms with hysteresis loops, which is associated with capillary condensation of nitrogen taking place in mesopores. The H2 hysteresis loop of MRP-1 indicates special ink-bottle-like mesopores with narrow opening, while H1 hysteresis loops of MRP-2 and MPR-3 generally suggesting cylindrical pores with more uniform size of resins[20]. As for MPR-3, it should have a certain amount of macropores (> 50 nm), as the isotherms showed no obvious adsorption saturation at large P/P_0 where fits the zone of multilayer adsorption. Quaternization didn't change the pore type of MPRs and QMPRs based on the same type of isotherms. However, the pore volumes of QMPR-2 and QMPR-3 drop significantly compared to MPRs, especially between the pore size of 30 and 50 nm (Fig. 2b). This could be primarily contributed by the swelling process, where it generally induce a 15–25% increase in bulk volume and squeeze mesopores of resins[21,22]. On the other hand, the swelling effect also result in higher surface area (Table 1) and higher amination efficiency, as the grafting of TMA may barely affect the pore structure of resin due to the small molecular size (0.66 nm) and

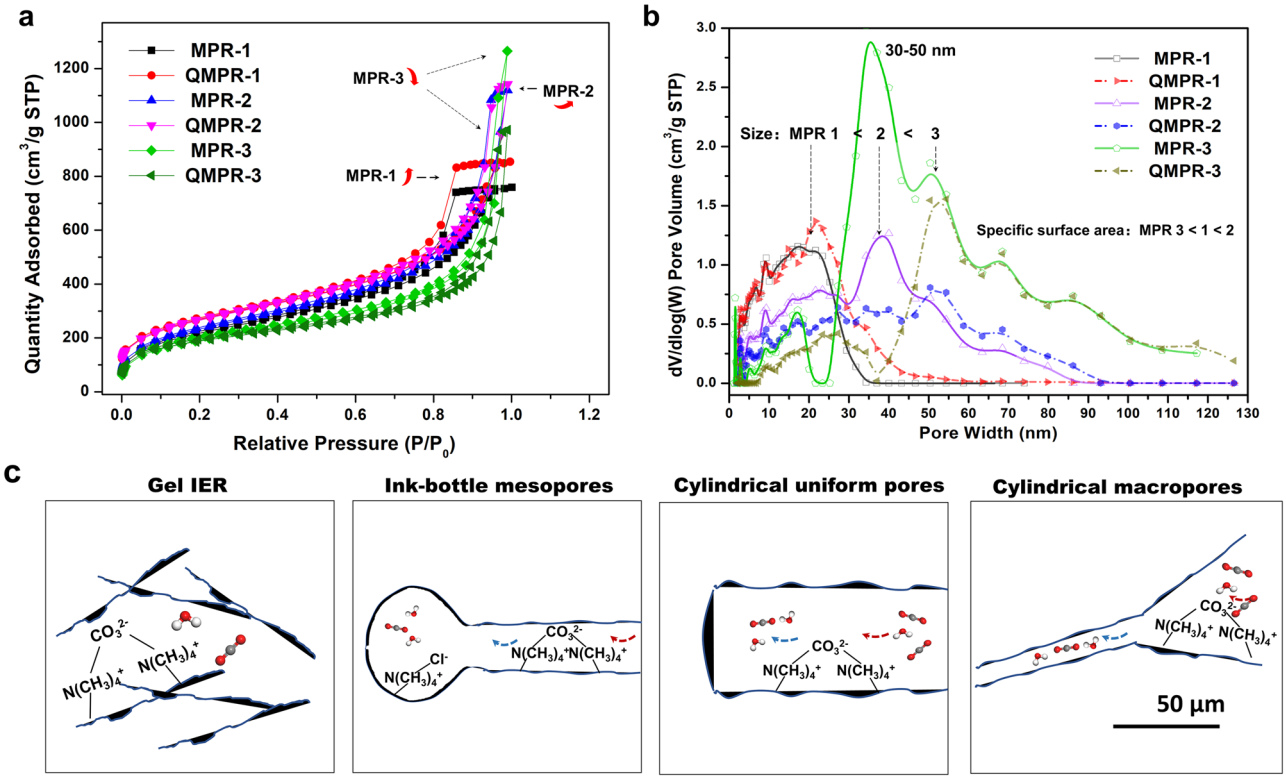

Figure 2. (**a**) N_2 adsorption–desorption isotherms. (**b**) Pore size distributions calculated by density functional theory (DFT). (**c**) Pore characteristic schemes of gel IER, ink-bottle mesoporous, cylindrical uniform pores and cylindrical macropores.

Resin samples	N (wt.%)	C/N	S_{BET} ($m^2\ g^{-1}$)	V_{DFT} ($cm^3\ g^{-1}$)	D_{DFT} (nm)
MPR-1	–	–	808	1.04	10.42
QMPR-1	1.30	55.95	975	1.24	11.51
MPR-2	–	–	864	0.92	21.64
QMPR-2	1.41	50.75	967	0.71	23.84
MPR-3	–	–	662	1.11	40.14
QMPR-3	1.39	51.97	636	0.62	46.68

Table 1. Summary of textural properties of resin samples. C and N: the weight content of carbon and nitrogen from element analysis, respectively. S_{BET} ($m^2\ g^{-1}$): the specific surface area by BET method; V_{DFT} ($cm^3\ g^{-1}$) and D_{DFT} (nm): the total pore volume and average pore size calculated by DFT method, respectively.

Adsorbents	ρ_i (mmol g^{-1})	Capacity (mmol g^{-1})			FG efficiency (%)	
		Q_N	Q_i	Q_{400ppm}	η_1 (Q_i/Q_N)	η_2 (Q_{400ppm}/Q_i)
QMPR-1	0.75	0.46	0.37	0.22	80.4	59.5
QMPR-2	0.93	0.50	0.46	0.28	92.0	60.9
QMPR-3	0.75	0.50	0.38	0.22	76.0	57.9

Table 2. Capacity and efficiency of polymeric resins for adsorption. ρ_i (mmol g^{-1}): ion charge density through Mohr titration; Q_N (mmol g^{-1}): CO_2 capacity calculated from N content; Q_i (mmol g^{-1}): CO_2 capacity calculated from ρ_i; Q_{400ppm}: experimental CO_2 capacity at 400 ppm. FG: the grafted functional group ($2[N(CH_3)_4]^+{\cdot}CO_3^{2-}$) of QMPR.

monolayer grafting[23]. The decreasing surface area of QMPR-3 compare to MPR-3 may be due to the combined effect of swelling and amination.

Quaternization with pore structure of MPRs. The CO_2 capacity of QMPRs can be predicted by nitrogen content (Q_N) or charge density (Q_c) through Eq. (1) below[13,24], which the results are listed in Table 2.

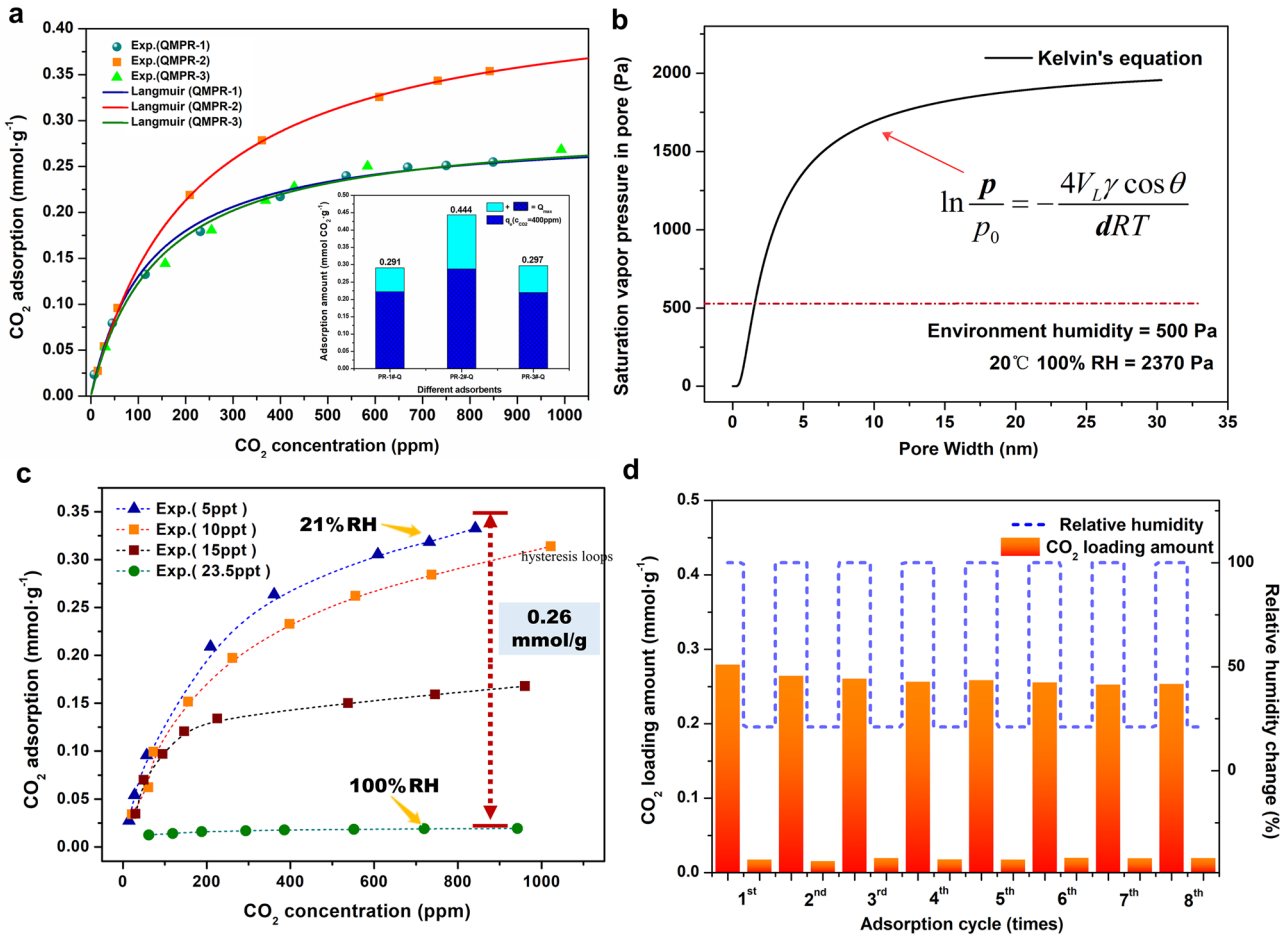

Figure 3. CO_2 adsorption performance and cycling of QMPRs. (**a**) Adsorption isotherms at 20 °C and 21% RH. (**b**) Local relative humidity of pores caused by capillary condensation of water. (**c**) Adsorption isotherms of QMPR-2 at different RH. A stable swing capacity of 0.26 mmol g^{-1} can be obtained by adsorbing at 21% RH and desorbing at 100% RH. (**d**) Multiple cycles for CO_2 adsorption by QMPR-2 at 400 ppm and desorbed at 100% RH.

$$CO_2 + (N^+)_2 \cdot CO_3^{2-} + H_2O = 2(N^+) \cdot HCO_3^- \quad (1)$$

The ion exchange efficiency of functional group (FG), η_1, is employed to measure the availability of QA group. Only the QA cations electrostatic interacting with carbonate ions are effective for CO_2 adsorption. Gel type ion exchange resins (IER) generally have a high η_1 of over 98%[25]. Compared with that, the relatively lower η_1 of QMPR should be due to the uneven distribution of QA groups inside the mesopores. Ion exchange for carbonate requires two QA cations with proper distance. Cation distance larger or shorter than the size of one carbonate molecule between two adjacent cations will result in increased potential energy of ion exchange[26]. For gel type IER, as illustrated in Fig. 2c, the cations are randomly distributed in the three-dimensional network of crosslinked polymer. The strong repulsion between cations will result in a uniform cation distance of about 0.8 nm for IER with charge density of 3.4 mmol g^{-1}, which provides proper space for counter anions with multivalence, e.g. carbonate, acetate, or phosphate anion[15,18]. During quaternization of QMPR, the diffusion of acyl group through micropores in gel type resins would have large resistance compared to diffusion through mesopores. The QA group would be concentrated inside the pores which can be indicated by the poor content of nitrogen, or large value of C/N. Uneven spatial distribution of cations, or cations with distance of far smaller or larger than the size of carbonate ion will result in poor ion exchange efficiency[26]. For QMPRs, the η_1 should also be related to the pore shape. Compared to QMRP-1 with ink-bottle pores and QMPR-3 with macropores, QMPR-2 with cylindrical mesopores is expected to have QA cations with more uniform spatial distance. This should be the reason why QMPR-2 has relatively higher ion exchange efficiency.

Mechanism of water effect on capacity of QMPRs. CO_2 adsorption isotherms of QMPR adsorbents are plotted in Fig. 3a, which exhibited Langmuir isotherm characteristics (Supplementary Fig. 3). No CO_2 adsorption is detected in MPRs (Supplementary Fig. 4). QMPR-2 exhibits the largest CO_2 capacity of 0.28 mmol g^{-1} under relative humidity (RH) of 21% and CO_2 concentration of 400 ppm, while QMPR-1 and QMPR-3 have relatively lower CO_2 capacity. This adsorption results consist with the ion exchange capacity of QMPRs. Table 2 shows that, for all the quaternized adsorbents, the functional group efficiencies at 400 ppm, η_2,

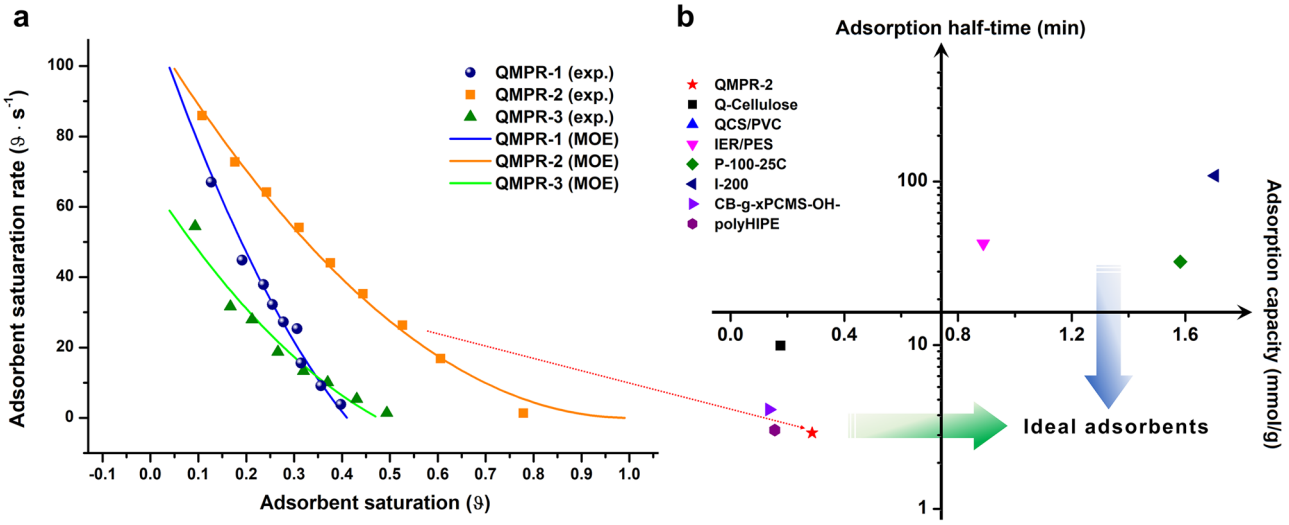

Figure 4. CO_2 adsorption kinetics and comparison among MSA adsorbents. (**a**) Adsorption kinetics of QMPRs at 20 °C and 21% RH. (**b**) Adsorption quadrantal diagram of developed MSA adsorbents for DAC.

are close to 60%. Although η_2 is larger than that of most solid amines[11,27], it is still lower than that of gel type IER[13]. From thermodynamic point of view, the functional group efficiency under a certain CO_2 partial pressure is determined by the equilibrium constant, which reflects the binding ability of adsorbents with CO_2. For moisture swing adsorbents, the CO_2 binding energy should be primarily affected by environmental humidity[24] and hydrophilicity of material[17]. Due to the hydrophilic feature of QA groups[27], QMPR has higher water sorption capacity compared to MPR (Supplementary Table 1). One can assume that the increased water content after amination is concentrated around the functional groups. Therefore, it is not surprising to find that QMPR and gel IER have similar hydrophilicity, or water content per functional group.

More influential effect goes to the capillary condensation of water taking place inside the pore channels, which changes the environmental humidity in local pores. The capillary condensation under equilibrium conditions is given by Kelvin's equation:

$$\ln \frac{p}{p_0} = -\frac{2V_L\gamma \cos\theta}{rRT} \tag{2}$$

V_L is the molar volume of water, γ is the surface tension of water, and R is the gas constant. For a hydrophilic surface (contact angle, $\theta, < 90°$), the saturation vapor pressure inside the pores (p), as a function of pore width (d) and temperature (T), is smaller than that in bulk phase (p_0). Condensation can, therefore, take place under higher relative humidity[28]. As illustrated in Fig. 3b, under water vapor partial pressure of 500 Pa at 20 °C (21% RH in ambient air), the local relative humidity in pores smaller than 10 nm could be over 30%. The increased number of water molecules surrounding by QA groups will increase the free energy of water dissociation for hydroxide ion and lead to decreased binding ability of adsorbents with CO_2[24]. The moisture swing adsorption property of QMPR-2 is depicted by the CO_2 adsorption isotherms at different relative humidity (Fig. 3c). By adsorbing 400 ppm CO_2 at 21% RH, and desorbing at RH of 100%, a stable swing capacity of 0.26 mmol g^{-1} can be obtained (cyclic adsorption shown in Fig. 3d).

Adsorption kinetics of QMPRs. Figure 4a demonstrates that CO_2 adsorption kinetics of QMPRs is governed by the surface area of adsorbent. QMRP-3, which owns the smallest surface area among adsorbents, has the lowest adsorption rate. QMPR-1 and QMPR-2 have similar surface area and their adsorption rates are also close at initial state. Meanwhile, it is interesting to find that the adsorption rate of QMPR-1 drops more rapidly with increased CO_2 saturation. This should be due to the special ink-bottle-like micro-pore structure as indicated by the hysteresis loop of QMRP-1. Previous isothermal studies[24] revealed that quaternary ammonium adsorbent will release part of hydrated water during CO_2 adsorption, e.g. 2.7 to 3.7 mol H_2O mol^{-1} CO_2. During CO_2 adsorption of QMPR-1, the released water could be gradually trapped by the ink-bottle-like microstructure. This would result in fast accumulation of humidity in local pores, and ultimately deteriorate its adsorption kinetics.

Adsorption half time of QMPRs, which is defined as the time to reach half of CO_2 capacity, could be calculated through a mixed 1,2-order equation[29] (Fitting result is shown in Supplementary Table 2). QMPR-2 exhibits an exciting feature of kinetics with half time of 2.9 min (Fig. 4b), which is the highest kinetics value reported among DAC adsorbents. Enhanced kinetics of MSA gives great opportunities to facilitate the deployment of direct air capture in large-scale carbon capture. Adsorption quadrantal diagram with two indicators of adsorption capacity and adsorption half-time is employed to evaluate the state-of-the-art MSA adsorbents for DAC. Due to the high extent of quaternization during sol–gel fabrication of commercial resin[24], the MSA adsorbents based on commercial quaternized resins generally have CO_2 capacity as high as 1.5 mmol g^{-1}, and are scattered

at quadrant I. Recently synthesized MSA adsorbents have high kinetics and located in quadrant III as they are bottom-up designed based on backbone with porous structure. The ideal MSA adsorbent, which has both high capacity and high kinetics, can be expected by grafting functional group into mesoporous resins during sol–gel fabrication process.

Discussion

The moisture swing separation process, which adsorb CO_2 at dry atmosphere and desorb CO_2 at high relative humidity, provides a promising approach to low cost CO_2 capture from air. In this work, the quaternary ammonium functional group was grafted onto mesoporous polymers to develop MSA adsorbent with high kinetics. In order to provide sufficient mass transfer channels for diffusion of functional group during grafting, Dichloromethane and methanol were selected as swelling agents as they can overcome steric hindrance and permeate reagents into active substitution sites at a sufficiently swelled state. The swelling effect also results in increased surface area and amination efficiency which are quite different from traditional amine functionalized adsorbents. Furthermore, cylindrical mesopores, which exhibits type IV isotherms with H1 hysteresis loops, are expected to have quaternary ammonium functional group with more uniform spatial distance and higher amination efficiency. The adsorbent synthesis employing proper swelling agents and polymer support with optimized mesoporous structure achieved adsorption half time of 2.9 min under atmospheric environment. This is the highest kinetics value reported among DAC adsorbents. Moreover, the behavior of water is significantly affected by mesopores, which further alters the binding energy of quaternary ammonium ion pair to CO_2. Mesopores have lower saturation vapor pressure according to Kelvin's equation capillary and have higher environmental humidity in local pores. The increased hydration water can distinctly decrease the binding energy of quaternary ammonium ion pairs to CO_2 through the Brønsted base mechanism. This can result in poor functional group efficiencies at 400 ppm, or moisture swing ability, compared to gel type ion exchange resin. Further improvement of MSA adsorbent with high capacity and kinetics can be expected by grafting quaternary ammonium into mesoporous matrix with hydrophobic groups.

Methods

Fabrication of QMPRs. Commercial nonpolar porous resins (XAD-4, XAD-16, and XAD-1180N, purchased from Aladdin, China) were pretreated by 0.1 M HCl, 5 wt.% NaOH and deionized (DI) water to remove the impurities. After dried at 60 °C under vacuum, 4.00 g mesoporous resin (MPR) sample was placed in a four-necked flask (equipped with constant pressure funnel, reflux condenser, thermometer, and mechanical stirring). 20 mL dichloromethane (CH_2Cl_2) was added as solvent and the mixture was stirred for 12 h to fully swell the microspheres. Chloroacetyl chloride (reagent) and powdered anhydrous aluminum chloride (Lewis catalyst) were slowly added to the mixture under N_2 protection (molar ratio of MPR to reagent to catalyst is 1:1:1). After 4.5 h room-temperature reaction, the mixture was suction-filtered and washed with tetrahydrofuran, 0.1 M HCl, and DI water in sequence, until chlorine ion could not be detected in the solution. The resulting light-brown microspheres were named as MPR-CA-1, MPR-CA-2, and MPR-CA-3, respectively.

The 4.00 g MPR-CA then swelled in 20 mL MeOH for 6 h at room temperature. Accompanied with 60 wt.% trimethylamine (TMA, 3.0 *e.q.* based on chloroacetyl chloride), the mixture was reacted in the flask with an oil bath (fitted reflux) pre-heated to 70 °C. After 4 h, the obtained resin microspheres (MPR-Cl) were packed in a column, washing with MeOH and DI water to remove the residuals. The obtained product was dried under vacuum at 60 °C for 12 h. After ion-exchange with 1 M Na_2CO_3 solution, the synthesized quaternary ammonium anion exchange mesoporous resins (QMPRs) were produced.

Characterization. Pore characteristics of MPRs and QMPRs were analyzed using N_2 adsorption/desorption isotherms (ASAP2020, Micromeritics, USA). Total pore volume was based on the adsorbed amount of N_2 at $P/P_0 = 0.99$. The specific surface area was calculated using Brunauer–Emmett–Teller (BET) method ($0.01 < P/P_0 < 0.1$), and pore-size distribution was obtained by density functional theory (DFT). Chemical structure of resin samples was identified by a Fourier transform infrared spectrometer (FTIR, Digilab BioRad FTS 6000 spectrometer, ATR mode), which scans from 4000 to 400 cm^{-1}. The element contents, including carbon, hydrogen, and nitrogen of resins, were determined though vario MAX cube and Elementar equipment. Surface morphology of resin samples were observed by a Hitachi SU-8010 scanning electron microscope (SEM) with an accelerating voltage of 20 kV. The Mohr titration was used to quantify the chloride ion amount in exchanging residue of QMPRs. By getting charge density (Q_c) of QMPR, an ideal CO_2 capacity can be calculated from it. Thus, it further gives the ion exchange efficiencies (η_1) of functional group (FG) and FG efficiencies at 400 ppm (η_2) of QMPRs.

CO2 adsorption measurements. CO_2 adsorption isotherms and kinetics were performed in a self-made system (Supplementary Fig. 5). CO_2 leakage was tested before each measurement. By repeatedly injecting 0.5 ml of CO_2 using syringe, the leakage rate was tested as 1.4×10^{-4} ppm s^{-1} under a CO_2 concentration difference of 500 ppm. This verifies that CO_2 leaking issue could be negligible compared to the injected amount.

Isothermal and kinetics models. 4.00 g QMPR was loaded in the reaction chamber, dried by ultra-high-purity (UHP) N_2 before adsorption. Relative humidity (RH) was controlled at 21% under 20 °C. CO_2 was injected into chamber repeatedly once adsorption equilibrium was reached. An isotherm related between CO_2 concentration and adsorbed amount can be obtained as:

$$Q_e = \frac{Q_{inj} - c_e V_s}{m_{ad} V_m} \tag{3}$$

where Q_e and Q_{inj} are CO_2 adsorbed and injected volume. c_e is the CO_2 concentration at equilibrium. V_s is the volume of the system (8 L). m_{ad} is the adsorbent weight. V_m is the molar volume.

Langmuir, Freundlich, and Temkin isotherm models are employed to fit the MSA equilibrium. These models can be reformed by linear relationship between monotonic function of Q_e and P.

$$\text{Langmuir isotherm:} \quad \frac{1}{Q_e} = \frac{1}{Q_{\max}} + \frac{1}{K' Q_{\max} P} \tag{4}$$

$$\text{Freundlich isotherm:} \quad \ln Q_e = A_1 + B_1 \ln P \tag{5}$$

$$\text{Temkin isotherm:} \quad Q_e = A_2 + B_2 \ln P \tag{6}$$

where Q_e and Q_{max} are CO_2 adsorbed amount at equilibrium and 100% saturation, respectively. A_1, B_1, A_2, and B_2 are adsorption parameters calculated by linear fitting. K' is the effective equilibrium constant of adsorption.

The normalized adsorption rate at a certain CO_2 concentration is determined by calculating the slope of $\theta_t \sim t$ curve. By measuring the CO_2 concentration (C_t) at time t, the saturation of adsorbent (θ_t) can be calculated as:

$$\theta(t) = \frac{Q_{inj} - C_t V_s}{Q_{\max}} \tag{7}$$

Pseudo-first-order (PFO), pseudo-second order (PSO), and mixed 1,2-order (MOE) rate models are employed to investigate the adsorption kinetics, which expressed as:

$$\text{PFO rate model:} \quad Q_t = Q_{e_1}(1 - e^{-k_1 t}) \tag{8}$$

$$\text{PSO rate model:} \quad Q_t = \frac{k_2 {Q_{e_2}}^2 t}{1 + k_2 {Q_{e_2}}^2 t} \tag{9}$$

$$\text{MOE rate model :} \quad Q_t = Q_{e_1}(1 - e^{-k_1 t}) + \frac{k_2 {Q_{e_2}}^2 t}{1 + k_2 {Q_{e_2}}^2 t} \tag{10}$$

$$f_2 = \frac{k_2 Q_{e_2}}{k_1 + k_2 Q_{e_2}} \tag{11}$$

where Q_t (mmol g^{-1}) is CO_2 adsorbed amount at time t, k_1 and k_2 are rate constants for PFO and PSO models, respectively. f_2 is the percentage of PSO equation in MOE rate model.

H_2O adsorption analysis. H_2O adsorption capacity of MPRs and QMPRs were obtained using a gravimetric method. Sample of resin (~ 1.00 g) were first dried in the chamber using UHP N_2, note m_d (g) as its dry mass. Humid N_2 (N_2 pass through humidity controller) was then introduced to the chamber, and record m_w (g) as the mass of sample saturated at a certain RH. This process was operated multiple times until m_w obtained from the electronic balance was stable. H_2O adsorbed amount of each sample, Q_w (mmol g^{-1}), was expressed as:

$$Q_w = \frac{1000(m_w - m_d)}{18 m_d} \tag{12}$$

Received: 15 May 2020; Accepted: 5 November 2020
Published online: 08 December 2020

References

1. Rogelj, J. *et al.* Mitigation pathways compatible with 1.5°C in the context of sustainable development. *Glob. Warm. 1.5°C. An IPCC Spec. Rep.* (2018).
2. National Academies of Sciences, Engineering, and Medicine Report. Negative emissions technologies and reliable sequestration: a research agenda. The National Academies Press. https://www.nap.edu/catalog/25259/negative-emissions-technologies-and-reliable-sequestration-a-research-agenda (2018).
3. Bui, M. *et al.* Carbon capture and storage (CCS): the way forward. *Energy Environ. Sci.* **11**, 1062–1176 (2018).
4. Sanz-Pérez, E. S., Murdock, C. R., Didas, S. A. & Jones, C. W. Direct capture of CO_2 from ambient air. *Chem. Rev.* **116**, 11840–11876 (2016).
5. Vicca, S. Global vegetation's CO_2 uptake. *Nat. Ecol. Evol.* **2**, 1840–1841 (2018).
6. Keppler, L. & Landschützer, P. Regional wind variability modulates the southern ocean carbon sink. *Sci. Rep.* **9**, 1–10 (2019).
7. D'Alessandro, D. M., Smit, B. & Long, J. R. Carbon dioxide capture: prospects for new materials. *Angew. Chem. Int. Ed.* **49**, 6058–6082 (2010).
8. Chen, Z. *et al.* Polyethylenimine-impregnated resin for high CO_2 adsorption: an efficient adsorbent for CO_2 capture from simulated flue gas and ambient air. *ACS Appl. Mater. Interfaces* **5**, 6937–6945 (2013).

9. Liu, F. Q. *et al.* Amine-tethered adsorbents based on three-dimensional macroporous silica for CO_2 capture from simulated flue gas and air. *ACS Appl. Mater. Interfaces* **6**, 4371–4381 (2014).
10. Kong, Y., Shen, X., Cui, S. & Fan, M. Facile synthesis of an amine hybrid aerogel with high adsorption efficiency and regenerability for air capture via a solvothermal-assisted sol-gel process and supercritical drying. *Green Chem.* **17**, 3436–3445 (2015).
11. Chaikittisilp, W., Kim, H. J. & Jones, C. W. Mesoporous alumina-supported amines as potential steam-stable adsorbents for capturing CO_2 from simulated flue gas and ambient air. *Energy Fuels* **25**, 5528–5537 (2011).
12. Rosenholm, J. M., Duchanoy, A. & Lindén, M. Hyperbranching surface polymerization as a tool for preferential functionalization of the outer surface of mesoporous silica. *Chem. Mater.* **20**, 1126–1133 (2008).
13. Wang, T., Lackner, K. S. & Wright, A. Moisture swing sorbent for carbon dioxide capture from ambient air. *Environ. Sci. Technol.* **45**, 6670–6675 (2011).
14. Shi, R. & Wang, Y. Dual ionic and organic nature of ionic liquids. *Sci. Rep.* **6**, 1–12 (2016).
15. Wang, T. *et al.* Designing moisture-swing CO_2 sorbents through anion screening of polymeric ionic liquids. *Energy Fuels* **31**, 11127–11133 (2017).
16. Song, J. *et al.* Quaternized chitosan/PVA aerogels for reversible CO_2 capture from ambient air. *Ind. Eng. Chem. Res.* **57**, 4941–4948 (2018).
17. Hou, C., Wu, Y., Wang, T., Wang, X. & Gao, X. Preparation of quaternized bamboo cellulose and its implication in direct air capture of CO_2. *Energy Fuels* **33**, 1745–1752 (2019).
18. Wang, T. *et al.* Spontaneous cooling absorption of CO_2 by a polymeric ionic liquid for direct air capture. *J. Phys. Chem. Lett.* **8**, 3986–3990 (2017).
19. Gao, B., Wang, L. & Du, R. Studies on chloroacylation reaction process of crosslinked polystyrene microspheres with ω-chloroacyl chloride as reagent. *J. Macromol. Sci. Part A Pure Appl. Chem.* **47**, 927–934 (2010).
20. Henderson, M. A. & Irwin, M. G. High humidity affects HemoCue microcuvette function. *Anaesth. Intensive Care* **23**, 407 (1995).
21. Zaleski, R., Krasucka, P., Skrzypiec, K. & Goworek, J. Macro- and nanoscopic studies of porous polymer swelling. *Macromolecules* **50**, 5080–5089 (2017).
22. Zhou, W. Q., Gu, T. Y., Su, Z. G. & Ma, G. H. Synthesis of macroporous poly(styrene-divinyl benzene) microspheres by surfactant reverse micelles swelling method. *Polymer (Guildf)* **48**, 1981–1988 (2007).
23. Lioe, H., Barlow, C. K. & O'Hair, R. A. J. How does acetylcholine lose trimethylamine? A density functional theory study of four competing mechanisms. *J. Am. Soc. Mass Spectrom.* **20**, 238–246 (2009).
24. Wang, T., Lackner, K. S. & Wright, A. B. Moisture-swing sorption for carbon dioxide capture from ambient air: a thermodynamic analysis. *Phys. Chem. Chem. Phys.* **15**, 504–514 (2013).
25. Pepper, K. W., Paisley, H. M. & Young, M. A. 833. Properties of ion-exchange resins in relation to their structure. Part VI. Anion-exchange resins derived from styrene-divinyl-benzene copolymers. *J. Chem. Soc* (Resumed), 4097–4105 (1953).
26. Shi, X. Study of a humidity-swing carbon dioxide sorbent (2017).
27. Shishatskiy, S., Pauls, J. R., Nunes, S. P. & Peinemann, K. V. Quaternary ammonium membrane materials for CO_2 separation. *J. Memb. Sci.* **359**, 44–53 (2010).
28. Morishige, K., Kawai, T. & Kittaka, S. Capillary condensation of water in mesoporous carbon. *J. Phys. Chem. C* **118**, 4664–4669 (2014).
29. Marczewski, A. W. Application of mixed order rate equations to adsorption of methylene blue on mesoporous carbons. *Appl. Surf. Sci.* **256**, 5145–5152 (2010).

Acknowledgements

This work is supported by the National Natural Science Foundation of China (No. 51676169) and Natural Science Funds for Distinguished Young Scholar of Zhejiang Province (LR19E060002).

Author contributions

T.W. conceived the research, X.R.W. and C.L.H. designed experiments. X.R.W., C.L.H. and J.L. analyzed the data. T.W. and X.R.W. wrote the manuscript. All authors discussed and commented on the manuscript.

Competing interests

The authors declare no competing interests.

Additional information

Supplementary Information The online version contains supplementary material available at https://doi.org/10.1038/s41598-020-77477-1.

Correspondence and requests for materials should be addressed to T.W.

Reprints and permissions information is available at www.nature.com/reprints.

Publisher's note Springer Nature remains neutral with regard to jurisdictional claims in published maps and institutional affiliations.